L.N. Ponomaryova [1], Yu.S. Dzyazko [2], Yu.M. Volfkovich [3], V.E. Sosenkin [3]

NANOPARTICLES OF ZIRCONIUM HYDROPHOSPHATE FRAMED WITH A WEAKLY-ACIDIC CATION-EXCHANGE POLYMER

[1] *Sumi National Agrarian University*
160 Gerasim Kondratiev Str., Sumy, 40021, Ukraine, E-mail: ponomarouva@gmail.com
[2] *V.I. Vernadskii Institute of General and Inorganic Chemistry of National Academy of Sciences of Ukraine*
32/34 Academician Palladin Avenue, Kyiv, 03142, Ukraine, E-mail: dzyazko@gmail.com
[3] *A.N. Frumkin Institute of Physical Chemistry and Electrochemistry of the RAS*
31 Leninskii Avenue, Moscow, 119071, Russia, E-mail: yuvolf40@mail.ru

Weakly acidic cation exchange resin was modified with nanoparticles of zirconium hydrophosphate. The materials were investigated with methods of standard contact porosimetry and transmission electron microscopy. Both non-aggregated nanoparticles (4–15 nm) and larger formations (from 250 nm to several microns) have been found. Single particles in clusters and channels of the polymer depress dissociation of carboxylic groups due to counter-ions (H^+) in electric double layer around the particles. This causes transformation of porous structure of the polymer: the contribution of micropores to total porosity increases. These additional selective sites provide stronger interaction of Brilliant Green molecules with the surface in comparison with the pristine polymer. Removal of the dye from deionized water and Ni(II) ions from water containing also hardness ions was studied under dynamic conditions. The composite shows higher break-through capacity than that of the pristine resin. The modifier also facilitates regeneration of the weakly acidic ion-exchanger.

Keywords: zirconium phosphate, organic-inorganic sorbent, cationic dye, nickel, nanoparticles, standard contact porosimetry, ion exchange, dye adsorption

INTRODUCTION

Sorbents that conjoin constituents of different nature are in a focus of attention. The combination of organic and inorganic ion exchangers gives a possibility to obtain sorbents with a wide spectrum of functional properties. As a rule, organic-inorganic materials are characterized by considerable exchange capacity and high rate of ion exchange. Their selectivity is more expressed than that for organic components. In comparison with inorganic sorbents, some composites show better granulometric properties that makes them suitable for the application in column under dynamic conditions [1]. Organic polymer also provides better mechanical properties for the sorbents. The organic-inorganic materials can be applied to water softening, separation and preconcentration of metal ions, nuclear separations, catalysis, redox systems, electrodeionization, hydrometallurgy, effluent treatment, production of ion selective electrodes and membranes. The composite sorbents are most often used for removal of toxic metal ions from water.

Organic-inorganic sorbents are divided into two classes based on interaction between organic and inorganic constituents [2]. In class I, organic and inorganic compounds are embedded with weak interactions, such as hydrogen bonding, van der Waals, π–π or weak electrostatic interactions between them. Regarding class II, these two components are bonded together through strong covalent or coordinative bonds.

Among the sorbents of the class II for recovery of toxic metal ions, such materials as organic-inorganic polymers [3] are developed intensively. As a rule, the polymers contain silanol groups attached to hydrocarbonaceous chains. Even Ni-form of chitosan, which is used for sorption of As(V)-containing anions, is considered to be a hybrid sorbent [4]. However, this relation is hardly true, since the material doesn't contain any functional inorganic groups. Other types of sorbents include inorganic matrix (silica [5–7], zirconia [8] or clay [9]) functionalized with organic fragments. Synthetic (for instance, double hydrated oxides [10]) and natural (clays [11–13], zeolites [13]) materials modified with surfactants can be related to

intermediate types of sorbents. They are capable to remove not only toxic inorganic ions, but also organic compounds. The sorbents possess high selectivity, but their sorption capacity is rather low comparing, for instance, with commercially available ion exchange resins. Moreover, chemical instability (sometimes even hydrolytic unsteadiness in acidic or alkaline media) narrows application field of the sorbents and complicates their regeneration.

The sorbents of the class I could be classified into nanocomposites, where: (i) nanoparticles (normally, inorganic ones) are embedded to other phase (usually to polymer) and distributed there homogeneously, (ii) both the polymer and inorganic constituents are in form of nanoparticles, (iii) nanoparticles of one constituent are coated with film of other constituent (core-shell structures). As an example, the inorganic nanoparticles inserted into ion exchange resins that are available commercially can be mentioned [14–19] (subclass i). The sorbents of second subclass involve nanoparticles that are distributed homogeneously in solid phase [20–24]. In this case, constituents are synthesized simultaneously or inorganic particles are inserted into reaction media where polymerization of organics occurs. At last, the subclass (iii) is formed by magnetic nanoparticles: their core is a magnetic material coated with functionalized polymer (shell) [25–28]. Particles consisting of polymer core and inorganic shell are considerably larger: with size of several microns and more [29, 30]. Some sorbents of this type are applied to controlled drug-delivery systems [29].

All sorbents of class II are characterized by high exchange capacity and significant selectivity. However, their destruction is possible under the influence of aggressive chemical reagents, which are necessary for desorption of toxic metal ions. Acidic solutions of rather high concentration are necessary for regeneration of sorbents loaded with toxic cations. This makes impossible application of magnetic nanoparticles as cation-exchangers, despite the fact that they were proposed for this purpose [25, 26].

From the point of view of chemical and mechanical stability, sorbents of subclass (i) are the most attractive. Weak bonds of the incorporated nanoparticles with the polymer surface play no key role, because the nanoparticles are retained in the ion exchange resin due to feature of its porous structure - the

pore system is an alternation of micro- and mesopores. Moreover, it is incorrect to talk about weak bonds in the case of incorporated aggregates and agglomerates of nanoparticles [14, 16–18, 31].

Earlier we used strongly acidic polymer matrix for modification with inorganic ion exchangers [14–18, 31]. However, weakly acidic ion exchange resins show better selectivity due to additional interaction of functional groups with sorbed ions. As expected, combination of weakly acidic polymer and inorganic constituents is capable to provide high selectivity towards toxic metal cations. The nanoparticles and their aggregates affect porous structure of the polymer constituent and, as a result, functional properties of the composites. The aim of the research was to establish an interrelation between porosity of the materials based on weakly acidic resins and their sorption behaviour.

EXPERIMENTAL

Following reagents were used for the investigation: NaOH, HCl, H_3PO_4, $ZrOCl_2 \cdot 8H_2O$, $NiSO_4 \cdot 7H_2O$ (lab or synthesis grade, Ukrkhimsyrie LTD), Brilliant Green (hydrogen sulphate) (Merck).

Such weakly acidic macroporous ion-exchanger as Dowex MAC 3 (Dow Chemical), which is based on polyacrylic matrix, was used for modification. Its ion exchange capability is provided by –COOH groups. This resin is used successfully for water purification [32]. Following characteristics are given by the company: total volume capacity –3.8 mmol cm^{-3} ($H^+ \rightarrow Na^+$), swelling of ion-exchanger bed – 70 %. Preliminarily the resin was washed with NaOH, HCl solutions, and deionized water as described elsewhere. It was found due to potentiometric titration that the pK of functional groups is 5.5.

The modification procedure was similar to [17, 18], it involved following stages: (i) swelling in deionized water, (ii) impregnation with 1 M $ZrOCl_2$ solution for 24 h followed by separation of solid and liquid, (iii) treatment with 1 M H_3PO_4 solution, separation of the solid and liquid, (iv) washing of the resin with deionized water up to pH 7 of the effluent, (v) drying at room temperature followed by treatment with ultrasound at 30 kHz using a Bandelin ultrasonic bath (Bandelin, Hungary), (vi) drying in a desiccator over $CaCl_2$ at 293 K down to constant

mass. Both the pristine and composite ion-exchangers were sieved, a fraction of 0.5–1 mm was taken for further study. Zirconium hydrophosphate was synthesized under similar conditions, the resin was not introduced into the reaction system. Fraction of 0.1–0.2 mm was used for investigation.

TEM images were obtained by means of a Jeol JEM 1230 transmission electron microscope (Jeol, Japan). Preliminarily the ion-exchangers were milled and treated with ultrasound.

A method of standard contact porosimetry (SCP) [33, 34], which had been accepted by the IUPAC [35], was applied to the pristine resin and composite as described, for instance, in [18]. Both the test sample and ceramic standard samples (for which the porosimetric curves are known) were dried under vacuum at 170 (standards) or 80 °C (ion-exchanger), further they were weighed separately. Then the sample was placed between two standards, vacuumed, impregnated with water and dried under vacuum. The set was disassembled periodically, its components were weighed. The state of capillary equilibrium was controlled for each point of the pore size distribution. The measurements were performed with constant mass of the samples. The equilibrium curve of relative moisture content was determined for the test sample. The curve is the dependence of amount of water in the studied sample on the liquid amount in the standards. Further pore size distributions were plotted as described in [33, 34]. Particle density of air-dried ion-exchangers was determined with a picnometer method [36].

Kinetics of BG adsorption was investigated under batch conditions. Initial content of the dye in its aqueous neutral solution, which was prepared using deionized water, was 5 mg dm^{-3} (0.01 mmol dm^{-3}). A series of weighted samples (0.2 g) were inserted to flasks, to which aliquots of the solution was added (20 cm^3). The process was carried out under intensive stirring by means of a Water Bath Shaker Type 357 (Elpan, Poland). After predetermined time, the solid and liquid from one flask were separated, at the end of the next period the solution was removed from the second flask and so on. Solutions were analyzed using a Shimadzu UV-mini1240 spectrophotometer (Shimadzu, Japan) at 625 nm. Adsorption capacity (*A*) was determined according to concentration difference.

In order to obtain adsorption isotherms, the solutions containing 1–7 mg·dm^{-3} (0.02–0.15 mmol dm^{-3}) of the dye was used, solution volume was 10 cm^3, sample mass was 0.2 g. Removal of BG from aqueous solution was carried out under dynamic conditions, initial concentration of the dye was 10 mg cm^{-3}. The diameter of the column was 0.7 cm, the volume of the ion-exchanger bed equaled 5 cm^3, solution velocity reached 5 cm^3 min^{-1}.

Ni(II) removal from tap water was also performed using ion exchange column, the conditions were the same. The solution contained (mmol dm^3): Ni(II) – 0.1, Ca(II) – 1.3, Mg(II) – 0.4. The effluent was analyzed by atomic absorption method using an S9 Pye Unicam spectrophotometer (Philips). After rapid increase of the content of Ni(II) ions in the effluent, the feeding solution was removed from the column, the ion-exchanger was washed with deionized water. Then 1 M H$_2$SO$_4$ solution was passed through the ion-exchanger bed, regeneration was carried out in this manner.

RESULTS AND DISCUSSION

Morphology of the composite was investigated using TEM microscopy (Fig. 1). As seen from the image of high resolution, the ion-exchanger contains spherical non-aggregated nanoparticles with size of ≈5–15 nm. Larger globular particles (from ≈250 to 600 nm) and irregular formations of micron size are seen in the image of lower resolution. The particles of different size can occupy one or another type of pores of the ion exchange polymer affecting its porous structure.

As a rule, a method of water adsorption isotherm is used to research the porous structure of ion exchange polymers [37]. This technique allows us to determine channels, clusters and partially voids between gel fields in polymer ion-exchange materials [17]. SCP data give information about all types of pores not only in rigid materials, but also in labile polymers [15–18, 31, 33, 38–41]. The mentioned techniques allow us to analyze only the polymer constituent of the composite, since no complete removal of water from the inorganic particles occurs at 353 K (i.e. under pretreatment conditions).

Main results of the porosimetric measurements are given in Table 1. As shown, modification reduces both total porosity and

microporosity of the polymer, however, particle density of the air-dried composite slightly increases. The last value is determined as $\frac{m_p + m_{in}}{v_c}$, where m_p and m_{in} are the masses of polymer and inorganic constituents in 1 cm³ of composite (v_c) respectively. Assuming no

significant increase of volume of the air-dried resin after modification, the $\frac{m_p}{v_c}$ term corresponds to particle density of the polymer. Thus, it is possible to estimate mass fraction of the modifier in volume unit of the composite.
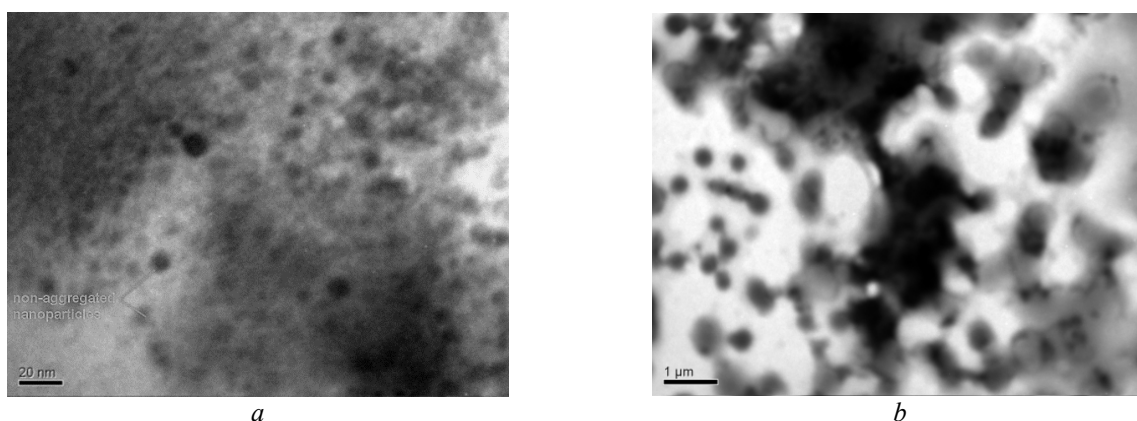
Fig. 1. TEM images of nanosized (*a*) and larger (*a, b*) particles of zirconium hydrophosphate in weakly acidic cation exchange resin

Table 1. Porosimetric measurements of the samples

Parameter	Pristine ion-exchanger	Composite ion-exchanger
*Particle density, g cm⁻³	1.18	1.29
*m		0.08
Porosity over weight, cm³ g⁻¹	1.68	1.47
Porosity over volume, cm³ cm⁻³	0.65	0.60
Specific surface over weight, m²g⁻¹	619	526
Specific surface over volume, m² cm⁻³	236	192
Micropore surface over weight, m²g⁻¹	365	344
Micropore surface over volume, m² cm⁻³	139	126
α	0.42	0.37
γ	0.56	0.90
n	4.31	3.94
L, nm	0.37	0.38

* The data were obtained by picnometer method

The data of porosimetric measurements for amorphous zirconium hydrophosphate were given earlier [41]. Total porosity of this inorganic ion-exchanger is 0.35, the contribution of microporosity is about 20 %, total specific surface area is about 100 m² g⁻¹. Porous structure involves pores of all size up to 1.6 μm. Mesopores with radius of 2.5 nm dominate.

Integral pore volume distributions are plotted in Fig. 2 *a* as dependences of the pore volume (*V*) on the logarithm of pore radius (*r*).

Fig. 2 *b* illustrates differential distributions. Since the equality of $\int_{\log r_1}^{\log r_2} \frac{dV}{d(\log r)} d(\log r) = \int_{lr_1}^{r_2} \frac{dV}{dr} dr$ is valid, the area of each peak corresponds to a contribution of certain pores to total porosity, $\frac{dV}{d(\log r)} = 2.3r\frac{dV}{dr}$.

The distributions reflect features of the porous structure of polymer ion exchange materials formed during swelling

[15–18, 31, 38–41]. As known, gel phase, which consists of hydrophilic parts of polymer chains, contains nanosized clusters and smaller channels between them, where functional groups are located. Since ions move mainly through clusters and channels, the latter are related to transport pores. Hydrophobic parts of polymer chains are placed in voids between gel fields (up to several hundreds nanometers). These voids and transport pores are formed only during swelling. The largest pores are structure defects with sizes bigger than 1 μm.

It is necessary to note that no shift of the stripes, which are related to mesopores, is observed for the composite comparing with the pristine resin. The peaks at $\log r = 0.5$ (nm) are related to clusters, their shoulders at $\log r \approx 0.25$ (nm) correspond to channels. The next stripe is about $\log r = 1.1$ (nm). As opposed to strongly acidic resins [15–18, 31, 41], especially flexible cation-exchanger [16], the mesopores are more disordered. The peaks at $\log r = 3.2–4.5$ (nm) are related to structure defects. Other difference between strongly and weakly acidic resins is higher volume of structure defects at $\log r = 3–3.2$ (nm). The largest pores are attributed to voids between grains, which are not taken into consideration. Dependent on their size, one or other types of incorporated particles can be located in channels, clusters, voids between gel regions and structure defects.

Fig. 1 *a* illustrates also the distributions of energy of water bonding with surface. "Bonded" water is located in channels (region I), so this region corresponds to the energy of water bonding (E, $E \geq 1700$ J mol^{-1}). This E value is less by approximately two orders of magnitude than the hydration energy of ions that is comparable with the energy of hydrogen bonds. Mobility of species is minimal in these pores. Zirconium hydrophosphate causes no significant decrease of bonded water in channels.

The region II corresponds to both bonded and free water in clusters ("boundary water"). In these pores the mobility of species is higher than that in channels, but lower comparing with pores filled with free water. Recalculation of the distribution for the composite as $\dfrac{V}{1-m}$ gives no coincidence for the curves for the pristine and

modified sorbent. It means that the modifier screens the clusters and decreases swelling.

The region III is related to free water in voids between gel fields and structure defects. The mobility of ions in these pores and in water outside the ion-exchanger is the same. However, no ion transport occurs through pores, which are free from functional groups despite the modifier particles there [18]. Zirconium hydrophosphate causes an increase of pore volume, a size of which is several tens microns. Moreover, these pores become larger.

Earlier the *α* and *γ* parameters have been proposed [16, 18] for establishing a relationship between structures of polymer and ion transport. The *α* parameter is a ratio of volumes of pores with functional groups and pores that are free from them. The *γ* value is a ratio of volumes of pores containing only bound water ($r < 1.5$ nm) and pores filled also with free water ($r > 1.5$ nm). These parameters were determined based on Figs. 2 *a, b*. As shown, modification reduces a contribution of clusters and channels to total porosity (see Table 1), but at the same time, the contribution of pores containing only bonded water increases. The parameters allow us to predict a decrease in the rate of ion transport through the polymer constituent.

Clusters and channels make main contribution to specific surface, S (Figs. 2 *c, d*). Here the shoulders at $\log r \approx 0.25$ (nm) for pore volume distributions (see Fig. 2 *b*) are seen as separate peaks. Isotherms of water adsorption (A_{H_2O}) are typical for materials containing different types of pores (Fig. 2 *e*). A slow growth of adsorption in a wide interval of P/P_s (here P is the pressure of water vapor, P_s is the pressure of saturated vapor) is related to micropores and partially to mesopores. The vertical region at $P/P_s \rightarrow 1$ is attributed to meso- and macropores.

According to thermodynamic Gregor's approach, a "concentrated solution" of counter-ions (H$^+$) and fixed ions (–COO$^-$) is diluted, when the ion-exchanger is in a contact with water [37]. This assumption is the closest to reality, when deionized water is used. Diffusion parts of intraporous double electric layers are overlapped in clusters and channels filling them completely. The tendency to "dilution" is assumed as a difference between the osmotic pressures inside and outside of ion-exchanger particles (swelling pressure). This term is

considered only in a framework of the Gregor's model, it is not related to swelling pressure of
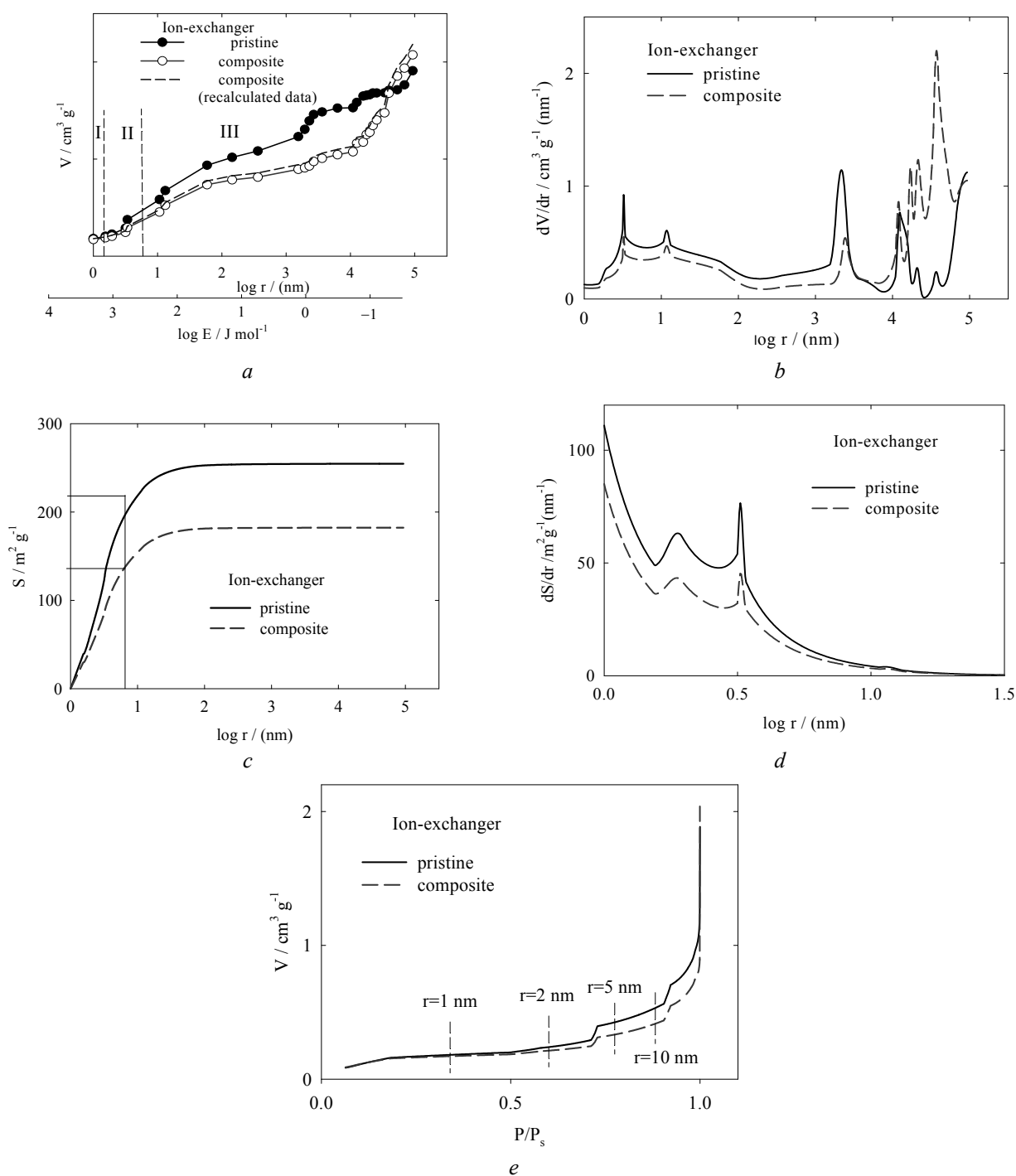
gel in a volume bounded with rigid walls.

a

b

c

d

e

Fig. 2. Pore volume (*a, b*) and energy (*a*) distributions, specific surface distributions (*c, d*) and isotherms of water adsorption (*e*). The distributions are given as integral (*a, c*) and differential (*b, d*) functions. Regions of bonded (I), boundary (II) and free (III) water are shown (*a*). Here the data for the composite were recalculated taking the polymer content into consideration. The surface distributions correspond only to meso- and macropores, here $S = 0$ at log $r = 0$ (*c, d*). The surface of micropores was calculated additionally. Pores of certain size are pointed by vertical dashed lines (*e*)

The isotherm for the composite is slightly shifted to the region of higher P/P_s values indicating higher swelling pressure comparing with the pristine weakly acidic resin. It was shown earlier that the particles of the inorganic ion-exchanger reduce swelling pressure in strongly acidic ion-exchanger, when they are located in gel phase [15, 16]. At the same time, coarse particles of micron size in structure defects increase the swelling pressure.

The amount of water molecules (n) in hydrate shells of counter-ions (H$^+$) of –COOH groups (hydration number) was calculated as

$$n = \frac{A_{H_2O}}{A_p V_{H_2O}} \qquad (2)$$

for the pristine ion-exchanger and

$$n = \frac{A_{H_2O}}{A_p V_{H_2O}(1-m)} \qquad (3)$$

for the composites. Here V_{H_2O} is the molar volume of water (0.018 cm^3·mmol^{-1}), A_p is the exchange capacity of the pristine polymer (2.3 mmol cm^{-3} at pH 6 for Na$^+$ ions, as has been found by means of potentiometric titration), A_{H_2O} is water adsorption in clusters and channels (in fact, the V value is expressed as cm^{3}cm^{-3}). Based on the data in Figs. 2 a and 2 b, the maximal size of clusters is about $\log r = 0.8$ (nm). In the case of the pristine polymer, the volume of water in clusters and channels is 0.18 cm^{3}cm^{-3} (see Fig. 2 a). Regarding the composite, $A_{H_2O} = 0.15$ cm^{3}cm^{-3}.

It is also possible to calculate a distance between carboxylic groups (L) [42]:

$$L = \sqrt{\frac{qS}{A_p F}} \cdot \qquad (4)$$

Here q is the electron charge, F is the Faraday constant, S is the specific surface area of clusters and channels. Following expression was used for the composite:

$$L = \sqrt{\frac{qS}{A_p F(1-m)}} \cdot \qquad (5)$$

The surface area was determined from Fig. 2 c (for clusters) and Table 1 (for channels)

and recalculated to the value over volume. As seen from the table, the L magnitudes are practically the same for the pristine and composite ion-exchangers.

In the case of strongly acidic resin, the volume of clusters and channels decreases under the influence of non-aggregated nanoparticles of zirconium hydrophosphate. Small content of the modifier also increases the α and γ parameters [15, 16, 18]. However, both the L [41] and n [15, 16] magnitudes increase despite screening of clusters and channels with non-aggregated nanoparticles. This happens due to stretching of pore walls: as a result, hydrated shells of counter ions becomes more complete [15, 16, 18]. Moreover, the particles in gel phase of the resin decrease Gregor's swelling pressure, when all the pores are filled with water (only the SCP method allows us to achieve these conditions) [15, 16].

Regarding the weakly acidic resin, it is possible to assume that the main amount of the inorganic ion-exchanger is located in the largest structure defects. Namely in these pores, large particles increase the swelling pressure [15] since they contain significant amount of dissociated functional groups. Indeed, size of the largest pores of the polymer constituent increases (see Fig. 2 b). From the formal point of view, the modifier inside the weakly acidic resin is similar to cross-linking agent in a polymer. As known, increasing in cross-linkage causes enhancement of swelling pressure [37].

The nanoparticles of more acidic zirconium phosphate in clusters and channels evidently depress dissociation of –COOH groups. This is due to high concentration of H$^+$ counter-ions in electric double layer around the particles. As a result, the A_p magnitude, which is used for calculations of hydrated number and distance between –COOH groups (expressions (3) and (5)), is overvalued. At the same time, the L and n magnitudes are undervalued. Unfortunately it is impossible to determine –COOH groups by method of potentiometric titration due to distorting effect of hydrophosphate groups, which are also dissociated in neutral media.

Porous structure of the polymer constituent affects adsorption capability of the composite, since pore size determines availability of adsorption centers. In order to fix this effect, BG adsorption was investigated. BG is related to cationic (basic) triphenylmethane dyes (Fig. 3)

with topological polar surface area of 2.3 nm^2 [43]. Thus, a radius of the molecule is ≈ 0.85 nm, its diffusion through the cluster-channel system is possible. Cationic and anionic dyes are capable to be adsorbed by hydrophobic [44] and hydrophilic [45] polymers as well as by inorganic materials [46, 47]. For example, the mechanism of adsorption on metal oxides involves not only electrostatic attraction, but also formation of hydrogen bonds between –OH groups and aromatic rings, as well as that of the bonds with nitrogen atoms and oxygen atoms [47]. It is expected that BG adsorption on the composite is affected by both hydrophilic and hydrophobic pores of the polymer as well as by pores of zirconium hydrophosphate.

Fig. 4 illustrates adsorption of BG over time. The models of chemical reactions, particle and film diffusion were applied to the data [37, 48] (Fig. 3, Table 2). For instance, the model of pseudo-first order is described by the Lagergren equation [48]:

$$\ln (A_\infty - A) = \ln A_\infty - K_1 \tau . \tag{6}$$

The model of pseudo-second order is [48]:

$$\frac{\tau}{A} = \frac{1}{K_2 A_\infty^2} + \frac{1}{A_\infty} \cdot \tau , \tag{7}$$

where τ is the time, A_∞ is the adsorption capacity at $\tau \to \infty$, A is the capacity at predetermined time, K_1 and K_2 are the rate constants. As follows from Table 2, the model of pseudo-first order is not suitable, since, the experimental and calculated A_∞ values are not similar. Diffusion models were found to be also not applicable. However, these values are close to each other for the model of pseudo-second order. Taking high correlation coefficients into consideration, this model can be applied. The composite demonstrates the highest adsorption capacity. However, the lowest reaction constant has been found for this ion-exchanger indicating the slowest adsorption.
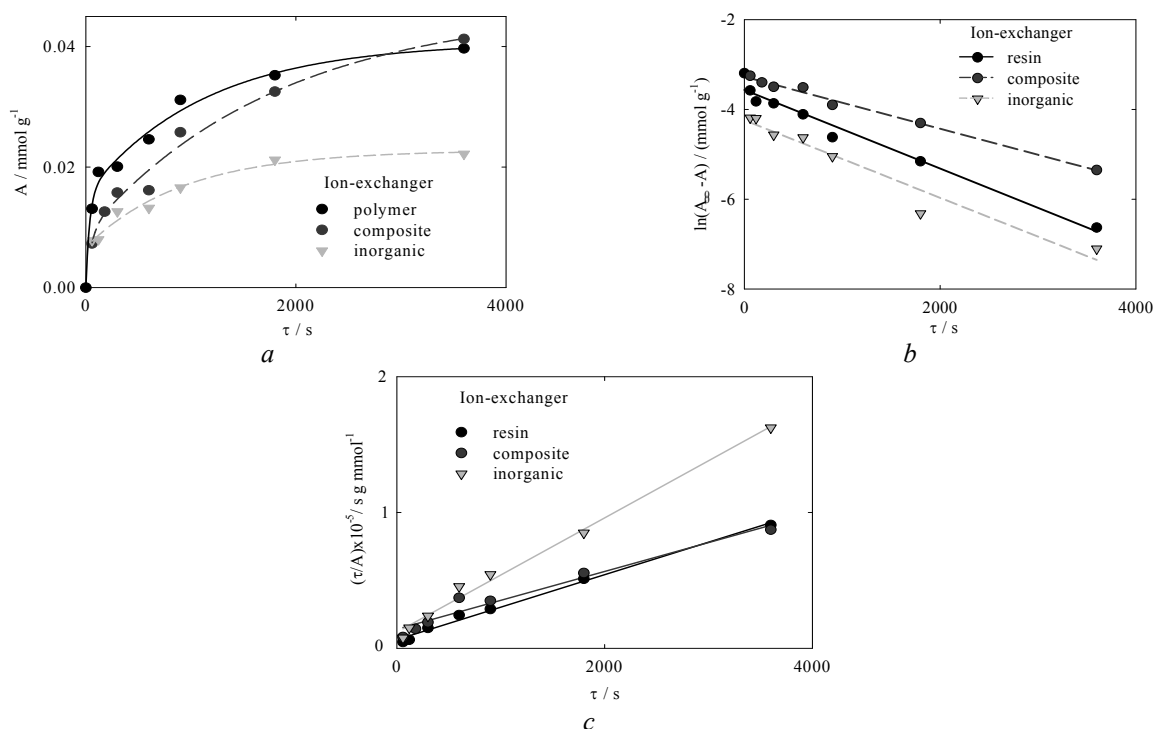

Fig. 3. Structure of Brilliant Green

Fig. 4. Adsorption capacity of the sorbents over time (*a*), application of the models of pseudo-first (*b*) and pseudo-second (*c*) orders

Table 2. Application of kinetic models to BG adsorption

Sample	$A_\maltese$, mmol g^{-1} (experimental value)	Pseudo-first order		Pseudo-second order		
		$A_\maltese$, mmol g^{-1} (calculated value)	R^2	$A_\maltese$, mmol g^{-1} (calculated value)	R^2	K_2, g mmol^{-1}s^{-1}
Pristine resin	0.041	2.18×10^{-4}	0.97	0.042	0.99	0.089
Composite	0.046	5.37×10^{-4}	0.99	0.047	0.96	0.032
Zirconium hydrophosphate	0.023	5.89×10^{-5}	0.95	0.023	0.99	0.161

Adsorption isotherms are given in Fig. 5. The isotherms are shown to demonstrate a growth of capacity followed by plateau. A number of models were applied to the data, the Langmuir model [49] was found to be the most suitable to fit the ascending sections of the curves. The equation is as follows:

$$\frac{1}{A} = \frac{1}{K_L A_{ml} C} + \frac{1}{A_{ml}}, \qquad (8)$$

where C is the equilibrium concentration, A_{ml} monolayer capacity, the K_L parameter characterizes the energy of interaction of molecules with surface. The A_{ml} values were determined also from the original data by extrapolation of the isotherms to infinity.

As seen from Table 3, the experimental and calculated A_{ml} magnitudes are rather close to each other. The polymer-based materials demonstrate stronger interaction of BG with surface and higher monolayer capacity than zirconium hydro-phosphate. However, modification of the resin with the inorganic modifier allows us to improve adsorption capability of the polymer despite screening of main part of pores with particles. When the initial BG concentration in the solution is 0.01 mmol·dm^{-3}, the capacity of the composite reaches 65 % of the maximal possible value (A_{max}). The A_{max} value is determined by dye content in the solution.

Let us compare the results with available literature data for cationic dyes adsorption on strongly acidic resin [45]. In this case, the initial dye concentration was 0.061 (Crystal Violet) and 0.074 (Basic Fluchsine) mmol·dm^{-3}. Adsorption capacity was 0.025 and 0.059 mmol·g^{-1} respectively. Since a ratio of masses of the solution and resin was 1:1, the adsorption capacity reached 41 and 80 % of the possible value. Thus, the adsorption capabilities of the weakly acidic and strongly acidic resins are comparable, the modifier improves BG adsorption sufficiently. This is evidently due to contribution of the particles inside pores of the polymer, which are free from functional groups. The interaction of BG with functional groups of zirconium hydrophosphate evidently slows adsorption down.
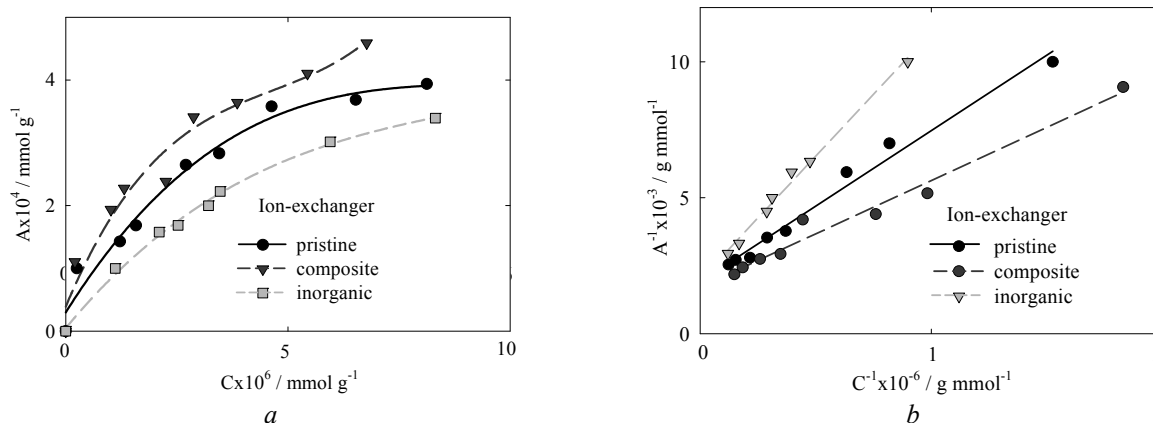

Fig. 5. Isotherms of BG adsorption in ordinary (*a*) and Langmuir (*b*) coordinates

Table 3. Application of Langmuir model to BG adsorption and Ni(II) removal from combining solution under dynamic conditions

Sample	BG					Ni(II)	
	experimental data		data calculated according to Langmuir model			break-through capacity, mg cm^{-3}	$\dfrac{A_{Ni}}{A_{Ca} + A_{Mg}}$ **
	$A_{ml}/$ mmol g^{-1}	A/A_{max} *	$A_{ml}/$ mmol g^{-1}	$K_L/$ g mmol^{-1}	R^2		
Pristine resin	4.11×10^{-4}	0.54	5.21×10^{-4}	3.81×10^{5}	0.98	19	2.9	0.57
Composite	4.89×10^{-4}	0.65	5.83×10^{-4}	4.36×10^{5}	0.97	91	6.0	0.49
Zirconium hydrophosphate	3.65×10^{-4}	0.42	5.05×10^{-4}	2.19×10^{5}	0.99	–	<0.1	0.19

The data were estimated for the initial BG concentration of 0.01 mmol·dm^{-3} (5 mg·dm^{-3})
** The data correspond to break-through capacity

Despite slower rate of BG adsorption on the composite, this material shows higher break-through capacity towards the dye comparing with the pristine resin (Fig. 6, see also Table 3). This is evidently due to higher adsorption capacity of the modified ion exchange resin. Passage through the column of the solution allows us to decrease the dye content in the effluent in 5.5–10 times. Improvement of water purification can be reached by optimization of adsorption process under dynamic conditions.
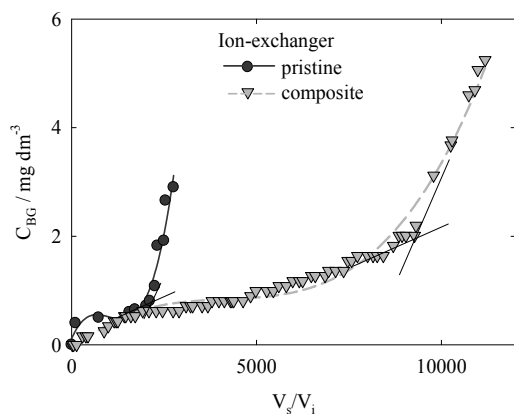

Fig. 6. Concentration of BG in the solution at the column outlet *vs* ratio of volumes of solution and ion-exchanger. Initial concentration of the dye was 10 mg·cm^{-3}

The composite demonstrates also the highest break-through capacity during removal of Ni(II) cations from the solution containing also hardness ions (Fig. 7, see also Table 3). Break-through capacity for one or other ion-exchanger is determined by content of dissociated functional groups [37]. Moreover, the break-through capacity depends on diffusion coefficient of sorbed ions. As shown above, the

modifier transforms porous structure of the polymer: a fraction of pores containing only bonded water increases. Simultaneously a fraction of pores that contain no functional groups (no ion transport is realized through these pores [18]) also increases. These factors slow down diffusion [16, 18]. Indeed, lower values of Ni(II) diffusion coefficients have been found for composite ion-exchangers than those for pristine ion exchange resin [41]. Thus, main reason of significant break-through capacity of the composite is high content of functional groups: the material contains not only –COOH groups, but also more acidic dihydrophosphate groups. The composite shows preferable sorption of Ni(II) ions in comparison with Ca^{2+} and Mg^{2+}.
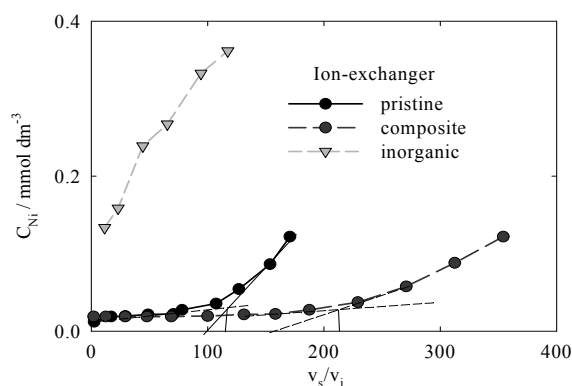

Fig. 7. Ni(II) content in the solution at the outlet of ion exchange column *vs* ratio of volumes of solution and ion-exchanger. The combining solution containing also hardness ions was desalinated

Incorporated zirconium hydrophosphate facilitates regeneration of the resin (Fig. 8). The initial content of sorbed ions in the composite was about 2 times higher in comparison with the

pristine polymer. However, the content of Ni(II) ions in the effluent is ≈ 17 times higher after regeneration of the composite (the initial Ni(II) content was 2 times higher in the modified resin comparing with the pristine polymer). Facile regeneration of the composite can be caused by location of particles in the largest pores of the polymers. The regenerating solution can be penetrated easy to these pores by passing the clusters-channels system.
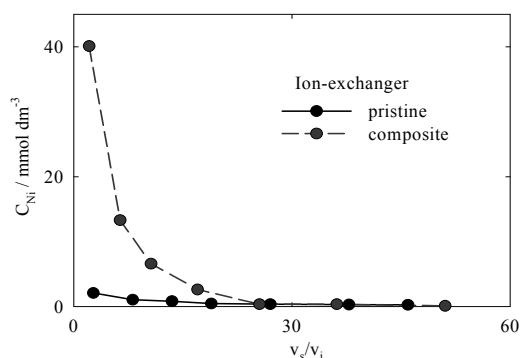

Fig. 8. Ni(II) content in the effluent at the outlet of ion-exchange column. Regeneration of the ion-exchangers after their loading with Ni(II) and hardness ions (see Fig. 7) was carried out

CONCLUSIONS

The modified weakly acidic cation-exchanger contains particles of zirconium hydrophosphate with size from 5 nm to several microns. From the formal point of view, the modifier inside the weakly acidic resin can be considered as a cross-linking agent, which increases swelling pressure. The nanoparticles are evidently located in pores containing –COOH groups, more acidic dihydrophosphate groups depress dissociation of functional groups of the polymer. As a result, porous structure of

the polymer constituent is transformed: a fraction of pores that contain only bonded water increases.

Since the smallest pores are responsible for selectivity, the enlargement of their fraction provides more preferable sorption of Ni(II) ions by the composite from the solution containing also Ca^{2+} and Mg^{2+}. This also improves interaction of Brilliant Green with the surface. As a result, the composite demonstrates higher adsorption capacity towards this dye than the pristine resin. Other reason of the improvement of dye adsorption can be appearance of additional adsorption sites in pores of the polymer that are free from –COOH groups. Phosphorus-containing groups of the modifier that is located there, provide additional BG uptake, since the mechanism of adsorption involves electrostatic attraction. It should be noted that the new sites slow down BG adsorption. However, the composite shows higher break-through capacity than that of the pristine resin.

The modifier also increases a fraction of pores containing no –COOH groups. Coarse particles of the modifier, which are located there, can be responsible for facile regeneration of the composite. This is due to easier penetration of the regenerating solution to these pores than to the system of nanosized clusters and channels.

Further development of composites based on weakly acidic resin is increase of the modifier content and control of particle size. The sorbent could be recommended for removal of toxic organic and inorganic ions from water. The advantages of the composite over commercial resins of the same type are higher adsorption and exchange capacity as well as facile regeneration.

Наночастинки гідрофосфату цирконію, армовані слабкокислотним катіонообмінним полімером

Л.М. Пономарьова, Ю.С. Дзязько, Ю.М. Вольфкович, В.Є. Сосєнкін

Сумський національний аграрний університет
вул. Герасима Кондратьєва, 160, Суми, 40021, Україна, ponomarouva@gmail.com
Інститут загальної та неорганічної хімії ім. В.І. Вернадського Національної академії наук України
просп. Академіка Палладіна, 32/34, Київ, 03142, Україна, dzyazko@gmail.com
Інститут фізичної хімії та електрохімії ім. О.Н. Фрумкіна РАН
Ленінський пр., 31, Москва, 119071, Росія, yuvolf40@mail.ru

Слабкокислотну катіонообмінну смолу модифіковано наночастинками гідрофосфату цирконію. Матеріали досліджено методами еталонної контактної порометрії та трансмісійної електронної мікроскопії. У фазі полімера знайдено як неагреговані наночастинки (5–15 нм), так і агрегати (від 250 нм до декількох мікрон). Наночастинки у кластерах та каналах полімера пригнічують дисоціацію карбоксильних груп, що зумовлено протиіонами (H^+) подвійного електричного шару навколо частинок. Це призводить до трансформації пористої структури полімера – внесок мікропор до загальної пористості зростає. Сформовані додаткові селективні центри обумовлюють більш сильну взаємодію з поверхнею молекул діамантового зеленого у порівнянні з немодифікованим полімером. Досліджено вилучення іонів Ni(II) з води, яка містить іони жорсткості, композит демонструє у два рази більшу ємність до проскока, ніж полімер. Модифікатор також полегшує регенерацію слабкокислотного іоніту.

Ключові слова: фосфат цирконію, органо-неорганічний сорбент, катіонний барвник, нікель, наночастинки, еталонна контактна порометрія, іонний обмін, адсорбція барвника

REFERENCES

1. Naushad M. Inorganic and composite ion exchange materials and their applications (Review). *Ion Exch. Lett.* 2009. **2**(1): 1.

2. Sanchez C., Julián B., Belleville P., Popall M. Applications of hybrid organic-inorganic nanocomposites. *J. Mater. Chem.* 2005. **15**(35–36): 3559.

3. Liu J., Ma Y., Xu T., Shao G. Preparation of zwitterionic hybrid polymer and its application for the removal of heavy metal ions from water. *J. Hazard. Mater.* 2010. **178**(1–3): 1021.

4. An B., Kim H., Park Ch., Lee S.-H., Cho J.-W. Preparation and characterization of an organic/inorganic hybrid sorbent (PLE) to enhance selectivity for As(V). *J. Hazard. Mater.* 2015. **289**: 54.

5. Awual Md.R., Miyazaki Yu., Taguchi T., Shiwaku H., Yaita T. Encapsulation of cesium from contaminated water with highly selective facial organic–inorganic mesoporous hybrid adsorbent di-*o*-benzo-*p*-xylyl-28-crown-8-ether silica. *Chem. Eng. J.* 2016. **291**: 128.

6. Awual Md.R., Hasanb Md.M., Shahat A. Functionalized novel mesoporous adsorbent for selective lead(II) ions monitoring and removal from wastewater. *Sens. Actuators B*. 2014. **203**: 854.

7. Shvets O., Belyakova L. Synthesis, characterization and sorption properties of silica modified with some derivatives of β-cyclodextrin. *J. Hazard. Mater.* 2015. **283**: 643.

8. Veliscek-Carolan J., Hanley T.L., Luca V. Zirconium organophosphonates as high capacity, selective lanthanide sorbents. *Sep. Purif. Technol.* 2014. **129**: 150.

9. Liang X., Xu Y., Tan X., Wang L., Sun Y., Lin D., Sun Y., Qin X., Wang Q. Heavy metal adsorbents mercapto and amino functionalized palygorskite: Preparation and characterization. *Colloids Surf. A*. 2013. **426**: 98.

10. Starukh G.M. Zn-Al layered double hydroxides for adsorption and photocatalytic removal of cationic dye. *Him. Fiz. Tehnol. Poverhni.* 2016. **7**(4): 379.

11. Liu C., Wu P., Zhu Y., Tran L. Simultaneous adsorption of Cd^{2+} and BPA on amphoteric surfactant activated montmorillonite. *Chemosphere*. 2016. **144**: 1026.

12. Ma L., Chen Q., Zhu J., Xi Y., He H., Zhu R., Tao Q., Ayoko G.A. Adsorption of phenol and Cu(II) onto cationic and zwitterionic surfactant modified montmorillonite in single and binary systems. *Chem. Eng. J.* 2016. **283**: 880.

13. Muir B., Matusik J., Bajda T. New insights into alkylammonium-functionalized clinoptilolite and Na-P1 zeolite: Structural and textural features. *Appl. Surf. Sci.* 2016. **361**: 242.

14. Perlova N., Dzyazko Y., Perlova O., Palchik A., Sazonova V. Formation of Zirconium Hydrophosphate Nanoparticles and Their Effect on Sorption of Uranyl Cations. *Nanoscale Res. Lett.* 2017. **12**: 209.

15. Dzyazko Yu.S., Perlova O.V., Perlova N.A., Volfkovich Yu.M., Sosenkin V.E., Trachevskii V.V., Sazonova V.F., Palchik A.V. Composite cation-exchange resins containing zirconium hydrophosphate for purification of water from U(VI) cations. *Desalin. Water Treat.* 2017. **69**: 142.

16. Dzyazko Yu.S., Volfkovich Y.M., Ponomaryova L.N., Sosenkin V.E., Trachevskii V.V., Belyakov V.N. Composite ion-exchangers based on flexible resin containing zirconium hydrophosphate for electromembrane separation. *J. Nanosci. Technol.* 2016. **2**(1): 43.

17. Dzyazko Yu., Ponomarova L., Volfkovich Yu., Tsirina V., Sosenkin V., Nikolska N., Belyakov V. Influence of zirconium hydrophosphate nanoparticles on porous structure and sorption capacity of the composites based on ion exchange resin. *Chemistry and Chemical Technology*. 2016. **10**(3): 329.

18. Dzyazko Yu.S., Ponomaryova L.N., Volfkovich Yu.M., Sosenkin V.E., Belyakov V.N. Polymer Ion-Exchangers Modified with Zirconium Hydrophosphate for Removal of Cd^{2+} Ions from Diluted Solutions. *Separ. Sci. Technol.* 2013. **48**(14): 2140.

19. Acelas N.Y., Martin B.D., López D., Jefferson B. Selective removal of phosphate from wastewater using hydrated metal oxides dispersed within anionic exchange media. *Chemosphere*. 2015. **119**: 1353.

20. Sharma G., Kumar A., Naushad M., Pathania D., Sillanpä M. Polyacrylamide @ Zr(IV) vanadophosphate nanocomposite: Ion exchange properties, antibacterial activity, and photocatalytic behavior. *J. Ind. Eng. Chem.* 2016. **33**: 201.

21. El-Naggar I.M., Hebash K.A., Sheneshen E.S., Abdel-Galil E.A. Preparation, characterization and ion-exchange properties of a new organic-inorganic composite cation exchanger polyaniline silicotitanate: Its applicationsfor treatment of hazardous metal ions from waste solutions. *Inorganic Chemistry*: *An Indian Journal*. 2014. **9**(1): 30.

22. Sharma G., Pathania D., Naushad Mu. Preparation, characterization, and ion exchange behavior of nanocomposite polyaniline zirconium(IV) selenotungstophosphate for the separation of toxic metal ions. *Ionics*. 2015. **21**(4): 1045.

23. Inamuddin, Shakeel Sh.Kh., Siddiqui W.A., Khan A.A. Synthesis, characterization and ion-exchange properties of a new and novel 'organic–inorganic' hybrid cation-exchanger: Nylon-6,6, Zr(IV) phosphate. *Talanta*. 2007. **71**(2): 841.

24. Qi H., Wang Sh., Liu H., Gao Y., Wang T., Huang Y. Synthesis of an organic–inorganic polypyrrole/titanium(IV) biphosphate hybrid for Cr(VI) removal. *J. Mol. Liq.* 2016. **215**: 402.

25. Ghasemi Sh., Ghorbani M., Ghazi M.M. Synthesis and characterization of organic–inorganic core–shell structure nanocomposite and application for Zn ions removal from aqueous solution in a fixed-bed column. *Appl. Surf. Sci.* 2015. **359**: 602.

26. Xu Y., Zhou Y., Ma W., Wang Sh., Li Sh. Functionalized magnetic core–shell $Fe_3O_4@SiO_2$ nanoparticles for sensitive detection and removal of Hg^{2+}. *J. Nanopart. Res.* 2013. **15**: 1716.

27. Shuang Ch., Pan F., Zhou Q., Li A., Li P. Magnetic Polyacrylic Anion Exchange Resin: Preparation, Characterization and Adsorption Behavior of Humic Acid. *Ind. Eng. Chem. Res.* 2012. **51**(11): 4380.

28. Zhao Y., Li J., Zhao L., Zhang Sh., Huang Y., Wu X., Wang X. Synthesis of amidoxime-functionalized $Fe_3O_4@SiO_2$ core–shell magnetic microspheres for highly efficient sorption of U(VI). *Chem. Eng. J.* 2014. **235**: 275.

29. Kamari Y., Ghiaci M. Preparation and characterization of ibuprofen/modified chitosan/TiO_2 hybrid composite as a controlled drug-delivery system. *Microporous Mesoporous Mater.* 2017. **234**: 361.

30. Zhang K., Cao M., Lou Ch., Wu Sh., Zhang P., Zhi M., Zhu Y. Graphene-coated polymeric anion exchangers for ion chromatography. *Anal. Chim. Acta.* 2017. **970**: 73.

31. Dzyazko Yu.S., Perlova O.V., Perlova N.A., Sazonova V.F., Ponomareva L.N., Volfkovich Yu.M., Palchik A.V., Trachevskii V.V., Belyakov V.N. Organic-inorganic ion-exchanger containing zirconium hydrophosphate for removal of uranium(VI) compounds from aqueous solutions. *Him. Fiz. Tehnol. Poverhni.* 2016. **7**(2): 119. [in Russian].

32. Dastgheib S.A., Knutson Ch., Yang Y., Salih H.H. Treatment of produced water from an oilfield and selected coal mines in the Illinois Basin. *Int. J. Greenhouse Gas Control.* 2016. **54**(2): 513.

33. Volfkovich Yu.M., Sosenkin V.E. Porous structure and wetting of fuel cell components as the factors determining their electrochemical characteristics. *Russ. Chem. Rev.* 2012. **81**(10): 936.

34. Volfkovich Yu.M., Bagotsky V.S. *Experimental methods for investigation of porous materials and powders, In: Porous materials and powders used in different fields of science and technology.* (London: Springer-Verlag, 2014).

35. Rouquerol J., Baron G., Denoyel R., Giesche H., Groen J., Klobes P., Levitz P., Neimark A. V., Rigby S., Skudas R., Sing K., Thommes M., Unger K. Liquid intrusion and alternative methods for the characterization of macroporous materials (IUPAC Technical Report). *Pure Appl. Chem.* 2012. **84**(1): 107.

36. Speight J.G. *Handbook of Petroleum Refining.* (Boca Raton: CRS Press, 2017).

37. Helfferich F. *Ion Exchange.* (New York: Dover, 1995).

38. Kononenko N., Nikonenko V., Grande D., Larchet C., Dammak L., Fomenko M., Volfkovich Yu. Porous structure of ion exchange membranes investigated by various techniques. *Adv. Colloid Interface Sci.* 2017. **246**: 196.

39. Berezina N.P., Kononenko N.A., Dyomina O.A., Gnusin N.P. Characterization of ion-exchange membrane materials: properties *vs* structure. *Adv. Colloid Interface Sci.* 2008. **139**: 3.

40. Kononenko N.A., Berezina N.P., Volfkovich Yu.M., Schkolnikov E.I. Investigation of the structure of ion exchange materials by calibrated porosimetry. *Journal of Applied Chemistry of the USSR.* 1985. **56**(10): 2029.

41. Dzyazko Yu.S., Ponomareva L.N., Volfkovich Y.M., Sosenkin V.E. Effect of the porous structure of polymer on the kinetics of Ni^{2+} exchange on hybrid inorganic–organic ionites. *Russ. J. Phys. Chem. A.* 2012. **86**(6): 913.

42. Volfkovich Y.M. Influence of the electric double layer on the internal interface in an ion exchanger on its electrochemical and sorption properties. *Soviet Electrochemistry.* 1984. **20**(5): 621.

43. PubChem - Open Chemistry Database. https://pubchem.ncbi.nlm.nih.gov/compound/90474287#section=3D-Conformer.

44. Eckenrode H.M., Jen S.H., Han J., Yeh A.G. Dai H.-L. Adsorption of a Cationic Dye Molecule on Polystyrene Microspheres in Colloids: Effect of Surface Charge and Composition Probed by Second Harmonic Generation. *J. Phys. Chem. B.* 2005. **109** (10): 4646.

45. Bayramoglu G., Altintas B., Arica M.Y. Adsorption kinetics and thermodynamic parameters of cationic dyes from aqueous solutions by using a new strong cation-exchange resin. *Chem. Eng. J.* 2009. **152**(2–3): 339.

46. Maheria K.C., Chudasama U.V. Sorptive removal of dyes using titanium phosphate. *Ind. Eng. Chem. Res.* 2007. **46**(21): 6852.

47. Abramian L., El-Rassy H. Adsorption kinetics and thermodynamics of azo-dye Orange II onto highly porous titania aerogel. *Chem. Eng. J.* 2009. **150**(2–3): 403.

48. Qiu H., LV L., Pan B.-C., Zhang Q.-J., Zhang W.-M., Zhang Q.-X. Critical review in adsorption kinetic models. *J. Zhejiang Univ. Sci. A.* 2009. **10**(5):716.

49. Rouquerol F., Rouquerol J., Sing H. *Adsorption by Powders and Porous Solids. Principles, Methodology and Applications.* (London-San Diego: Academic Press Publishing, 1999).